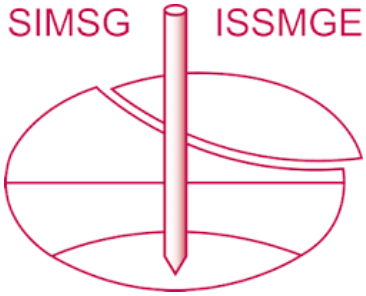
INTERNATIONAL SOCIETY FOR
SOIL MECHANICS AND
GEOTECHNICAL ENGINEERING



This paper was downloaded from the Online Library of the International Society for Soil Mechanics and Geotechnical Engineering (ISSMGE). The library is available here:

https://www.issmge.org/publications/online-library

This is an open-access database that archives thousands of papers published under the Auspices of the ISSMGE and maintained by the Innovation and Development Committee of ISSMGE.

The paper was published in the proceedings of the 6th International Conference on Geotechnical and Geophysical Site Characterization and was edited by Tamás Huszák, András Mahler and Edina Koch. The conference was originally scheduled to be held in Budapest, Hungary in 2020, but due to the COVID-19 pandemic, it was held online from September 26th to September 29th 2021.

Deformation Behavior of Volcanic Sandy Soil Shirasu by Elastoplastic Constitutive Model

Mizuki Hira
Kagoshima University, Kagoshima, Japan, hira@agri.kagoshima-u.ac.jp

Kentaro Yamamoto
Nishinippon Institute of Technology, Fukuoka, Japan, kyama@nishitech.ac.jp

ABSTRACT: This study is aimed for the description of the deformation behavior of volcanic sandy soil Shirasu for reclamation and embankment, by the elastoplastic constitutive equation adopting the subloading surface model with the rotational hardening. And also test results for the isotropic consolidation and the monotonic/cyclic loading-unloading compression with several lateral stresses under the drained conditions for various initial void ratios are reported. Further, the simulation by the constitutive equation based on the extended subloading surface model is compared with the test results. High applicability of the constitutive equation for the prediction of mechanical behavior of Shirasu for a geo-material at the construction site in the southern Kyushu is verified by the comparison.

Keywords: Shirasu soil; stress-strain relation; elasto-plasiticity; constitutive equation; subloading surface model

1. Introduction

Volcanic sandy soil "Shirasu" is widely distributed at the neighboring parts of Caldera in the southern Kyushu, Japan. It has a considerable apparent cohesion in the undisturbed state as a soft rock but loses cohesion in the disturbed state as sand, whilst the disturbance is caused even by a submersion. Therefore, serious damages, e.g. the collapse of slopes, the breaking of embankments, etc. have often gone into headlines at heavy rainfalls. Hence, the prediction of the deformation behavior of this soil is of quite importance from the viewpoint of practical engineering for the prevention of disasters.

2. Elasto-plastic constitutive equation based on the subloading surface concept

In this section the subloading surface model and its application to soils (Hashiguchi et al.(1997,1998) is reviewed briefly, which will be later applied to the analysis of the deformation behavior of Shirasu. Let it be assumed that the stretching $\mathbf{D}$ is additively decomposed into the elastic stretching $\mathbf{D}^e$ and the plastic stretching $\mathbf{D}^p$, i. e.

$$\mathbf{D}=\mathbf{D}^e+\mathbf{D}^p, \tag{1}$$

where the elastic stretching $\mathbf{D}^e$ is given by

$$\mathbf{D}^e=\mathbf{E}^{-1}\overset{\circ}{\boldsymbol{\sigma}}. \tag{2}$$

$\boldsymbol{\sigma}$ is the *Cauchy stress* and $(^\circ)$ indicates the Jaumann rate and E is the elastic modulus.

Normal-yield and Subloading Surfaces are

$$f(\hat{\boldsymbol{\sigma}},\boldsymbol{H})=F(H)\ (\hat{\boldsymbol{\sigma}}\equiv\boldsymbol{\sigma}-\boldsymbol{\alpha}), \tag{3}$$

$$f(\bar{\boldsymbol{\sigma}},\boldsymbol{H})=RF(H), \tag{4}$$

where $\bar{\boldsymbol{\sigma}}\equiv\boldsymbol{\sigma}-\bar{\boldsymbol{\alpha}}\ (=R(\boldsymbol{\sigma}_y-\boldsymbol{\alpha}))$,

$$\bar{\boldsymbol{\alpha}}\equiv\boldsymbol{s}-R(\boldsymbol{s}-\boldsymbol{\alpha})=\boldsymbol{s}-R\hat{\boldsymbol{s}}\ \ (\bar{\boldsymbol{\alpha}}-\boldsymbol{s}=R(\boldsymbol{\alpha}-\boldsymbol{s})). \tag{5}$$

H and $\boldsymbol{H}$ are the isotropic and the anisotropic hardening variables. $\bar{\boldsymbol{\alpha}}$ on or inside the subloading surface is the conjugate point of the reference point $\boldsymbol{\alpha}$ on or inside the normal-yield surface, $\boldsymbol{\sigma}_y$ on the normal-yield surface is regarded as the conjugate point of the current stress $\boldsymbol{\sigma}$ on the subloading surface, $\boldsymbol{s}$ is the similarity-center of their two surfaces and R is the similarity-ratio of the surfaces, whilst its evolution rule is given by

$$\dot{R}=U\left\|\boldsymbol{D}^p\right\| \ \text{for}\ \boldsymbol{D}^p\neq\boldsymbol{O},\ U=-u\ln R, \tag{6}$$

where u is the material constant and $(\dot{\ })$ denotes the material-time derivative.

Translation Rule of Similarity-Center:

$$\overset{\circ}{\boldsymbol{s}}=c\left\|\boldsymbol{D}^p\right\|\frac{\tilde{\boldsymbol{\sigma}}}{R}+\overset{\circ}{\boldsymbol{\alpha}}+\frac{1}{F}\Big\{\dot{F}-\mathrm{tr}\Big(\frac{\partial f(\hat{\boldsymbol{s}},\boldsymbol{H})}{\partial\boldsymbol{H}}\overset{\circ}{\boldsymbol{H}}\Big)\Big\}\hat{\boldsymbol{s}}$$

$$,\ \tilde{\boldsymbol{\sigma}}\equiv\boldsymbol{\sigma}-\boldsymbol{s}, \tag{7}$$

where c is the material constant.

Plastic Stretching:

$$\boldsymbol{D}^p=\lambda\bar{\boldsymbol{N}}=\frac{\mathrm{tr}(\bar{\boldsymbol{N}}\overset{\circ}{\boldsymbol{\sigma}})}{\bar{M}_p}\bar{\boldsymbol{N}}=\frac{\mathrm{tr}(\bar{\boldsymbol{N}}\boldsymbol{E}\boldsymbol{D})}{\bar{M}_p+\mathrm{tr}(\bar{\boldsymbol{N}}\boldsymbol{E}\bar{\boldsymbol{N}})}\bar{\boldsymbol{N}}, \tag{8}$$

where $\bar{\boldsymbol{N}}\equiv\dfrac{\partial f(\bar{\boldsymbol{\sigma}},\boldsymbol{H})}{\partial\boldsymbol{\sigma}}\Big/\left\|\dfrac{\partial f(\bar{\boldsymbol{\sigma}},\boldsymbol{H})}{\partial\boldsymbol{\sigma}}\right\|$, (9)

$$\bar{M}_p\equiv\mathrm{tr}\Big[\bar{\boldsymbol{N}}\Big(\Big\{\frac{F'}{F}h-\frac{1}{RF}\mathrm{tr}\Big(\frac{\partial f(\bar{\boldsymbol{\sigma}},\boldsymbol{H})}{\partial\boldsymbol{H}}\boldsymbol{h}\Big)+\frac{U}{R}\Big\}\bar{\boldsymbol{\sigma}}+\bar{\boldsymbol{a}}\Big)\Big]$$

$$, \tag{10}$$

$$F'\equiv dF/dH,\ h\equiv\dot{H}/\lambda,\ \ \boldsymbol{h}\equiv\overset{\circ}{\boldsymbol{H}}/\lambda,$$

$$\bar{\boldsymbol{a}}\equiv\overset{\circ}{\bar{\boldsymbol{\alpha}}}/\lambda=R\boldsymbol{a}+(1-R)\boldsymbol{z}-U\hat{\boldsymbol{s}},\ \boldsymbol{a}\equiv\overset{\circ}{\boldsymbol{a}}/\lambda, \tag{11}$$

$$\boldsymbol{z} \equiv \frac{\overset{\circ}{\hat{\boldsymbol{s}}}}{\lambda} = c\tilde{\boldsymbol{\sigma}} + \boldsymbol{a} + \frac{1}{F}\left\{F'h - \mathrm{tr}\left(\frac{\partial f(\hat{\boldsymbol{s}},\, \boldsymbol{H})}{\partial \boldsymbol{H}}\boldsymbol{h}\right)\right\}\hat{\boldsymbol{s}} \,. \tag{12}$$

Loading Criterion:

$$\boldsymbol{D}^p \neq \boldsymbol{0} :\ \mathrm{tr}(\bar{\boldsymbol{N}}\boldsymbol{E}\boldsymbol{D}) > 0,\ \ \boldsymbol{D}^p = \boldsymbol{0} :\ \mathrm{tr}(\bar{\boldsymbol{N}}\boldsymbol{E}\boldsymbol{D}) \leq 0 \,. \tag{13}$$

Material function of Shirasu soil

The functions $f(\bar{\boldsymbol{\sigma}},\, \boldsymbol{H})$ and $f(\hat{\boldsymbol{s}},\, \boldsymbol{H})$ are given for soils as

$$f(\bar{\boldsymbol{\sigma}},\, \boldsymbol{H}) = \bar{p}(1 + \bar{\chi}^2) \quad , \tag{14}$$
$$f(\hat{\boldsymbol{s}},\, \boldsymbol{H}) = \hat{p}_s(1 + \hat{\chi}_s^2) \,,$$

where $\bar{p} \equiv -(\mathrm{tr}\,\bar{\boldsymbol{\sigma}})/3$, $\bar{\boldsymbol{\sigma}}^* \equiv \bar{\boldsymbol{\sigma}} + \bar{p}\boldsymbol{I}$,

$$\hat{p}_s \equiv -(\mathrm{tr}\,\hat{\boldsymbol{s}})/3 \quad , \tag{15}$$

$$\bar{\chi} \equiv \| \bar{\boldsymbol{\eta}} \| / \bar{m} \,,\ \hat{\chi}_s \equiv \| \hat{\boldsymbol{\eta}}_s \| / \hat{m}_s \,, \tag{16}$$

$$\bar{\boldsymbol{\eta}} \equiv \bar{\boldsymbol{Q}} - \boldsymbol{\beta} \,,\ \bar{\boldsymbol{Q}} \equiv \bar{\boldsymbol{\sigma}}^* / \bar{p} \,,\ \hat{\boldsymbol{\eta}}_s \equiv \hat{\boldsymbol{Q}}_s - \boldsymbol{\beta} \,,$$
$$\hat{\boldsymbol{Q}}_s \equiv \hat{\boldsymbol{s}}^* / \hat{p}_s \,,\ \hat{\boldsymbol{s}}^* \equiv \hat{\boldsymbol{s}} + \hat{p}_s \boldsymbol{I} \,, \tag{17}$$

$$\bar{m} = 2\sqrt{6}\sin\phi / (3 - \sin\phi \sin 3\bar{\theta}_\eta \,), \tag{18}$$
$$\hat{m}_s = 2\sqrt{6}\sin\phi / (3 - \sin\phi \sin 3\hat{\theta}_s \,),$$

$$\sin 3\bar{\theta}_\eta \equiv -\sqrt{6}\,\mathrm{tr}\,\bar{\boldsymbol{\eta}}^3 / \| \bar{\boldsymbol{\eta}} \|^3 \,, \tag{19}$$
$$\sin 3\hat{\theta}_s \equiv -\sqrt{6}\,\mathrm{tr}\,\hat{\boldsymbol{\eta}}_s^3 / \| \hat{\boldsymbol{\eta}}_s \|^3$$

and f is the material constant. The anisotropic hardening variable $\boldsymbol{H}$ is selected as the rotational hardening variable $\boldsymbol{\beta}$. The evolution rule of rotational hardening is given by

$$\overset{\circ}{\boldsymbol{\beta}} = b_r \left\| \boldsymbol{D}^{p*} \right\| \| \bar{\boldsymbol{\eta}} \| [\{2\sqrt{6}\sin\phi_b / (3 - \sin\phi_b \sin 3\bar{\theta}_\eta)\}\, \bar{\boldsymbol{\eta}} / \| \bar{\boldsymbol{\eta}} \| - \boldsymbol{\beta}], \tag{20}$$

where b_r and f_b are material constants. The isotropic hardening variable H is given by

$$\dot{H} = -\varepsilon_v^p (\equiv -\mathrm{tr}D^p), \quad H = \int \dot{H} \,, \tag{21}$$

where ε_v^p is the plastic volumetric strain. The isotropic hardening/softening function F is given by

$$F = F_0 \exp\{H / (\rho - \gamma)\}, \tag{22}$$

where F_0 is the initial value of F. r and g are the slope of the normal-consolidation and the swelling curve, respectively, in the space (ln$p$, ln$v$) (p: pressure, v: volume). The material constants and initial values are selected as follows.

3. Comparison with test data

3.1. Physical properties and test procedure

Shirasu sample used for the tests was taken from Kirishima city, Kagoshima Prefecture. The physical properties are shown in Table 1.

Table 1. Physical properties of Shirasu

Grading Sand		77	%
Silt		20	%
Clay		3	%
Coefficient of uniformity	U_c	38.9	
Coefficient of curvature	U_c'	3.84	
Specific gravity of soil particles	G_s	2.43	

The gravel fraction of Shirasu consists mainly of pumice and a small amount of derived rock fragments such as andesite. The particles are considerably angular. Coarse fragments are subangular to angular, and the shape becomes angular as the grain size becomes finer, and only thin, flat and angular particles are observed in the finest fraction. Most of the fragments are volcanic glass; its surface texture generally looks smooth. On the other hand, the pumice has frothy structure and its surface is very rough. This is the reason why the Shirasu has small density compared with other sandy soils (Haruyama(1969,1985,1997). The water content was adjusted to be 15% after natural drying in the laboratory and sieving through the net of 2.0mm meshes. The specimens were compacted using a rammer in a cylindrical mold of 50mm in diameter and 125mm in height, so as to give a specified initial density. Furthermore, the layer and compaction numbers were set in accordance with the form of Proctor's equation to give three kinds of density, and thus initial void ratio was prepared to be three levels 0.83, 0.95 and 1.01.

In order to measure volumetric change precisely, specimens saturated as much as possible (Skempton's B-value > 0.95) are prepared by vacuum procedure [Rad et al.(1984)] by which the effective isotropic stress $\boldsymbol{\sigma}$ =4.9**I** kPa (0.05 kgf/cm^2) is applied to specimens at the beginning of tests.

3.2. Material parameters for simulation

The material constants, and the initial value F_0 are determined so as to fit the test result of isotropic consolidation illustrated in Fig. 1. The Poisson's ratio ν is obtained by the value of and the inclination of the initial rising part of stress-strain curve in the triaxial compression test results. The parameter u in the evolution rule of the normal-yield ratio R is determined from the curvature of the stress-strain curve in the transitional state from the elastic to the normal-yield state, while it is smaller for looser samples. The stress ratio at the stress on the normal-yield surface in which the outward-normal vector loses the component of hydrostatic axis changes only slightly. Especially, it is fixed independent of the rotation in the yield surface of the original Cam-clay model. The angle of internal friction in the critical state can be determined approximately from the stress ratio in the residual state. The limit-angle of the rotational hardening and the parameter br controlling the rate of rotational hardening are

determined so as to supplement the degree of hardening in the test result with the deviatoric deformation. The material parameters used in the simulation are prepared appropriately, where F_0 stands for the values of F in the initial state e ($\boldsymbol{\sigma}$ =4.9 **I** kPa) of calculation.

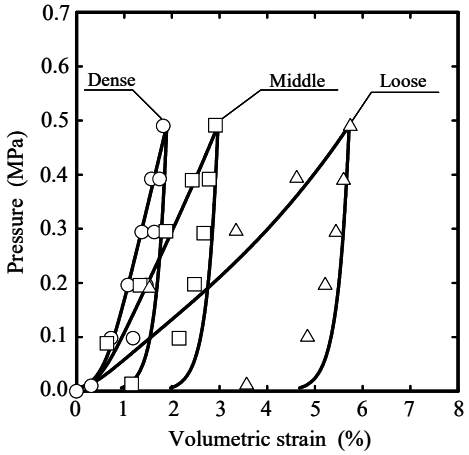


Fig. 1. Relations of volumetric strain versus pressure for isotropic loading-unloading processes.

3.3. Comparison of theory and experiment

All the calculations are started from the unique isotropic effective stress state $\boldsymbol{\sigma}$ =4.9**I** kPa and thus in the triaxial tests the isotropic consolidation test is performed until the prescribed confining pressure. All the calculated results are depicted by solid lines.

Isotropic loading-unloading consolidation behavior for dense, middle and loose samples is shown in Fig.1. A fairly good prediction of the volumetric strain-pressure curves is attained. The differences of the volumetric strain with changes in the initial void ratio are realistically simulated by the theory, whilst the plastic deformation is predicted properly even in the subyield state.

The relationships of the deviatoric stress and the volumetric strain versus the axial strain under the drained triaxial compression are depicted in Fig. 2 for dense, middle and loose samples subjected to four levels of confining pressure. The stress-strain curves of dense samples exhibit a peak in the deviatoric stress, whilst the curvature of the curves decreases with the increment of the confining pressure. The predicted stresses after peak are higher than the stresses in the test results. It might be caused by the shear band formation in the test samples as will be described in the end of this section. On the other hand, the curves of loose samples do not exhibit a peak despite of the confining pressure. The volumetric strain-axial strain curves also agree well with the test data. The phenomenon observed in the test results of dense samples that the maximum ratio of the volumetric strain increment to the axial strain increment is realized at the peak state of axial stress is predicted exactly by the theory.

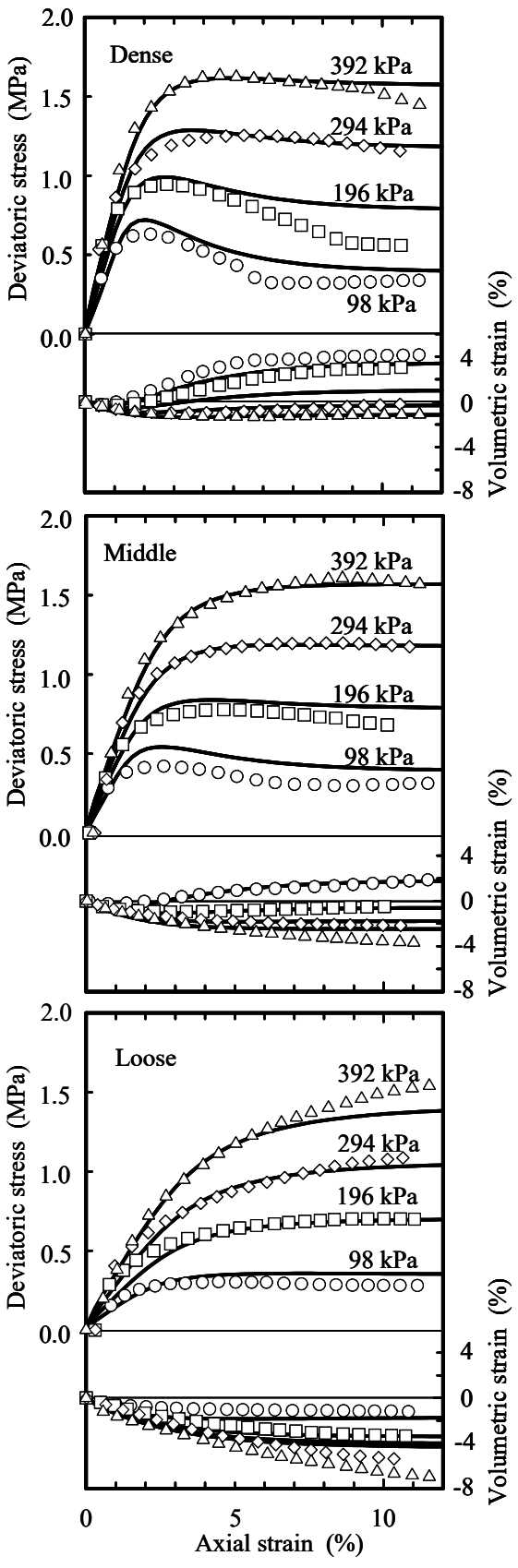


Fig.2. Relations of axial strain versus deviatoric stress, axial strain versus volumetric strain for drained triaxial compression test of dense, middle and loose samples.

This phenomenon has been widely known as the experimental fact for over-consolidated soils as has been written even in the classical literature of Taylor, whilst it was suggested by Newland and Alley from the test of dense, middle and loose samples strain versus volumetric strain for drained triaxial compression micromechanical aspect that “When sliding just begins, the shear stress and rate of volumetric expansion reach maximum values, since at this state the sliding contact angles of soil particles to the shear plane are at their maximum”.

3.4. Mechanical features of Shirasu soil

The deformation behavior of compacted Shirasu was predicted here by the elastoplastic constitutive equation. The prediction would have been attained historically first in this paper. Therefore, it is difficult yet to found mechanical features of Shirasu definitely. In the present situation the following mechanical features of Shirasu from the viewpoint of constitutive equation might be indicated comparing with those of clays (Topolnicki (1990), Asaoka (1997)), and sands (Noda et al. (2001)).

1. Particles of Shirasu have size similar to that of sands but are quite angular leading to cohesion by compaction. Therefore, in general speaking, Shirasu exhibits deformation behavior of clays and/or sands depending on the test conditions. Besides, the compacted Shirasu sample exhibits rather brittle behavior and thus would lead to shear band formation causing an apparent softening more intense than softening predicted as a constitutive property. It would be the reason for the difference of stress-strain curves after peak stress in calculated and test results as seen in Fig. 2.
2. After the initial unloading stage, the value of axial strain is very small, the plastic strain component of Shirasu is also small.
3. The void ratio is large in the order of clays, Shirasu and sands, and thus (inclination of normal-consolidation line) is larger (easily compressed and fragile) and evolution rate of the normal-yield ratio u is smaller (easily deforms plastically) in this order.
4. The elastic deformation is substantially caused by the deformation of soil particles themselves, and thus inclination of swelling (elastic consolidation) curve is not so different between clays, Shirasu and sands.

4. Conclusions

The description of deformation behavior of Shirasu soil by the elastoplastic constitutive equation is studied adopting the subloading surface model with the rotational hardening. The predicted results by the constitutive equation were compared with some test data of compacted Shirasu samples for the isotropic consolidation and the triaxial monotonic and cyclic compression under the drained condition for normal- and over-consolidated states for various initial void ratios subjected to various levels of lateral stress.

Here, severe calculations were performed starting from unique isotropic stress state and using each unique set of values of material parameters depending on dense, middle and loose samples. The capability of reproducing real deformation behavior of this volcanic sandy soil was verified in this comparison.

Further, the constitutive equation is limited to the prediction of monotonic loading behavior. In order to predict the cyclic loading behavior of Shirasu, the extended subloading surface model with kinematic hardening variable can be shown a good agreement with test results. The elastoplastic constitutive equation by the extension of the subloading surface model is effective in predicting a mechanical ratcheting behavior for soils. However, tested samples are limited to artificially compacted samples and thus the comparison with undisturbed natural samples would be desirable in order to confirm the capability.

References

[1] Haruyama, M.: Effect of water content on the shear characteristics of granular soils such as Shirasu. Soils and Foundations. 9 (3), pp. 35-57, 1968.

[2] Hashiguchi, K. and Ueno, M.: Elastoplastic constitutive laws of granular materials, Constitutive Equations of Soils. (Proc. 9th ICFSME, Spec. Sess. 9), Tokyo, JSSMFE, and Tokyo, 73-82, 1977

[3] Rad, N.S. and Clough, G.W.: New procedure for saturating sand specimens. J. Geo. Eng. Div. (ASCE). 110, pp.1205-1218, 1984.

[4] Haruyama, M.: Drained deformation-strength characteristics of loose Shirasu (volcanic sandy soil) under three dimensional stresses. Soils and Foundations.25 (1), pp. 65-76.1985

[5] Topolnicki, M.: An elasto-plastic subloading surface model for clay with isotropic and kinematic mixed hardening parameters. Soils and Foundations. 30 (2), pp.103-113,1990

[6] Asaoka, A., Nakano, M. and Noda, T.: Soil-water coupled behavior of heavily over consolidated clay near/at critical state. Soils and Foundations. 37 (1), pp.13-28,1997

[7] Haruyama, M.: Deformation characteristics of highly compressible sand “Shirasu”. Soils and Foundations.17 (1), pp.39-51,1997

[8] Hashiguchi, K. and Chen, Z.-P. : Elastoplastic constitutive equation of soils with the subloading surface and the rotational hardening. Int. J. Numer. Anal. Mech. Geomech. 22,pp.197-227,1998

[9] Noda, T., Nakano, M., Mizuno, K. and Takeuchi, H.: A soil-water coupled analysis on the effect of improvement of a loose sandy ground by cylindrical cavity expansion. Soils and Foundations. 41 (4), pp.113-123 (in Japanese),2001